sustainability

Article

Assessment of the Mechanisms of Summer Thermal Environment of Waterfront Space in China's Cold Regions

Fan Fei [1], Yan Wang [1,2,*] and Xiaoyun Jia [3]

[1] School of Architecture, Tianjin Chengjian University, Tianjin 300384, China; ff_tcu@163.com
[2] State Key Laboratory of Green Building in Western China, Xi'an University of Architecture & Technology, Xi'an 710055, China
[3] Dalian Institute of Architectural Design and Research, Dalian 116021, China; 15522928112@163.com
* Correspondence: wang.y@tcu.edu.cn; Tel.: +86-22-23085067

Abstract: Water is an essential part of the urban ecosystem and plays a vital role in alleviating urban heat island (UHI) problems. The contribution toward UHI mitigation made by bodies of water needs to be ascertained to establish waterfront thermal environment construction standards. In this study, the thermal environment of the waterfront space of Tianjin in the cold regions of China was the research object. Through a survey including 141 valid questionnaires and the field measurement of four typical waterfront spaces in Tianjin, the thermal demand characteristics of recreational use for the waterfront environment and the influence of water on microclimate are discussed, supplemented by results from low-altitude infrared remote sensing technology, which was mainly used to obtain a wider range of infrared thermal images with higher accuracy. To improve the urban heat island effect and the quality of the ecological environment, this paper used outdoor thermal environment simulation software to quantitatively analyze the thermal environmental impact of outdoor public activity spaces around the representative urban body of water and proposes the optimization scheme of the waterfront space's thermal environment. The results show that, based on the factors of water itself, the most economical water width was 70–80 m, and the cooling effect intensity of water had an essential correlation with the distance between the measured site and the water center. In terms of the environmental factors around the water, when the green lawn of the waterfront space was 12 m and the water shore's geometric form was S-shaped, this could improve the cooling effect of water significantly. Waterfront activity spaces should focus on thermal comfort on the east and south water shores. It is expected that this study could provide practical implications and useful guidance for the planning and design of urban waterfront space in China's cold regions.

Keywords: waterfront space; thermal environment; WBGT; low-altitude infrared remote sensing; CFD simulation

Citation: Fei, F.; Wang, Y.; Jia, X. Assessment of the Mechanisms of Summer Thermal Environment of Waterfront Space in China's Cold Regions. *Sustainability* **2022**, *14*, 2512. https://doi.org/10.3390/su14052512

Academic Editor: Constantinos Cartalis

Received: 29 December 2021
Accepted: 20 February 2022
Published: 22 February 2022

1. Introduction

Rapid urbanization has led to a high concentration of city dwellers. According to the predictions of the United Nations and the World Bank, the proportion of the world's population living in urban areas will grow rapidly in the 21st century, which is expected to reach 66% by 2050 [1]. Rapid and sustained urbanization promotes the improvement of transportation facilities and the development of tourism and trade. Simultaneously, it also puts great pressure on local natural resources and the ecological environment [2,3]. A high density of urban population, closely situated high-rise buildings, and an impervious underlying surface affect the urban climate environment. This is characterized by urban heat island (UHI) issues, which result in high-temperature heatwaves in summer, an increase in the number of deaths from heatstroke, and an increase in refrigeration energy consumption and greenhouse gas emissions [4–6]. Such manmade and meteorological factors are not conducive to the sustainable development of urban ecosystems [7–10].

The urban surface environment is highly heterogeneous. In meteorology, the occurrence of small-scale near-stratigraphic climate conditions, caused by the heterogeneity of the underlying surface and human activities, is called a microclimate [11–14]. Microclimates have strong adjustability, which directly affects the comfort of urban residents' daily life. In recent years, the impact of underlying landscape on microclimate has attracted more and more attention [15–18]. The "oasis effect" of water and greenery, and the negative impact of artificial underlying surfaces, such as buildings and impermeable pavement, on ambient temperature have been studied [19–22]. Therefore, many mechanisms have been proposed to alleviate UHI, such as natural water bodies, greenery (urban green spaces, vertical greening, and green roofs), and changing urban geometry form. First of all, as the underlying surface of an urban cold source, water plays an essential part in alleviating the effect of UHI [23–26]. Some scholars chose urban lakes as their research object, while other scholars chose urban rivers [27–31]. The most widely used method was field measurement, although lacking comprehensiveness and integrity of data [32–37]. It was found that the water had an obvious "cold island" effect on the surrounding area. At present, the research on the "cold island" effect of urban water mainly focuses on two aspects. Based on the factors of the water itself, the influence of water area changes, the shape index, and depth on the cooling and humidification effect of water was explored. Starting with the environmental factors around the water, aiming at analyzing the building layout and height, building retreat distance, urban form, and other factors, combined with CFD and other numerical simulation methods, these studies explore the impact of various factors on the "cold island" effect exerted by bodies of water. Cheng et al. [38] found that the cooling distance from a lake varied according to the underlying surfaces, such as forest (462.5 m), hard surfaces (400 m), grassland (326.5 m), and bare land (262.5 m). However, the nighttime temperature of the waterfront space will inevitably be higher in summer, which will enhance the UHI effect [31]. Meanwhile, with the refinement of computer numerical simulation, current research on influencing factors, such as greenery and urban form, is more in-depth [39–41]. Greenery is another promising strategy for mitigating thermal stress through the complementary mechanisms of shadowing, evapotranspiration, and air-movement shielding [42,43]. Anjos et al. [44] reported that the cooling effect of urban green spaces was mainly affected by greenery structure, size, shape, types, and spatial distribution. De Jesus et al. [45] showed that the air temperature of a vertical greening wall was 2.5–2.9 °C lower than that of the bare wall in Madrid, Spain. Wong et al. [46] revealed that the green roof on a low-rise building contributed a cooling effect to both the building and its surrounding environment in Singapore. However, the mitigation effect of green roofs varies with building height. Last, but not least, the connection between urban geometry form and UHI is well-established, as this can create canyons discharging heat and pollutants [47,48]. Urban geometry is quantified by the aspect ratio, street orientation, and sky view factor (SVF), as usual. Takebayashi [49] discussed the finding that the shading effect of a tall building in north–south street canyons had less impact on solar gain than that in east–west streets, as measured in Tokyo. However, the cooling effect of urban geometry is greatly affected by cloud cover, and it has been found that cloudy skies cause a substantial decrease in the cooling rates of urban canyons [50].

Although previous research has focused on extensive discussions regarding the UHI mitigation effects of bodies of water, greenery, and urban forms in isolation, some essential aspects of the waterfront's thermal environment have not yet been properly addressed in the long term. More and more research has been conducted into the construction of public environments planned around urban water through place modeling, but the lack of improvement in the environment around water, from the perspective of human needs, leads to poor thermal comfort in the public spaces around water. Most of the methods for studying the thermal comfort of waterfront spaces are measured in terms of the ground, and there is less research on the cooling effect of water based on low-altitude remote sensing. Most studies only consider the combination of urban squares and urban water to improve the thermal comfort of waterfront spaces, and a lack of quantitative analysis of the impact of typical urban bodies of water on the thermal sensations experienced by the surrounding people. Researchers have mainly focused on the cooling effect of large-scale rivers or lakes, and have proposed scientific guidance for urban planning, but have neglected quantitative research into different micro-scale water body types alleviating the UHI, especially in China's cold regions.

Against this background, the wide waterfront space in Tianjin, which has no tall buildings nearby, is selected as the research object because of Tianjin's urban development. This area is taken as a typical example of China's cold regions, based on the occurrence of water-surrounding environment construction and the poor thermal comfort of the waterfront space. This paper aims to explore the relevant environmental factors influencing the public space around the water from the perspective of thermal comfort, put forward the possibility of low-altitude infrared remote sensing technology to mitigate the UHI effect, establish the thermal demand characteristics of waterfront residents, and utilize thermal environment simulation software to quantitatively analyze the influencing characteristics of water on the microclimate of the waterfront's public activity space, which helps in the development of strategies proposed for waterfront construction, based on land use and evaluation standards. The outcomes of this study will contribute to alleviating the UHI effect in urban micro-scale waterfront spaces, and further improve thermal comfort for urban residents. However, the recommended strategy of utilizing the cooling effect of water may not be fully applicable in other climatic regions, such as in hot and humid areas, due to the high humidity.

2. Study Area and Methods

2.1. Study Region

Tianjin is at 116°43′–118°40′ E and 38°34′–40°15′ N, located in the northern part of the North China plain. It is an important city in the Bohai Bay area, situated in the cold region of China (Figure 1) [51]. Plains in cold regions have longer winters, which are cold and dry. The summer is hot, but it is not as humid as the hot and humid regions of the south [52]. Tianjin is rich in water resources and has high economic strength, but there are several problems regarding the development of waterfront space in terms of landscape design, including the single-form riverbank design, the simple and monotonous landscape along the river, the area not meeting people's needs, and the lack of hydrophilicity. In this study, many rivers in the Tianjin area were investigated and analyzed, and the most suitable urban water area was chosen as the research object. Tall buildings throw shadows and change the surrounding wind field, which affects the thermal environment to a certain extent. Therefore, the actual conditions of the environment surrounding the water should be comprehensively considered when selecting the research site. The study sites were almost all typical urban planar water (lake) and linear water (river) scenarios. The representative waterfront public space survey objects in Tianjin were at site 1 (a circular lake, Figure 2a), site 2 (an annular lake, Figure 2b), site 3 (a river of north–south orientation, Figure 2c), and site 4 (a river of east–west orientation, Figure 2d). In the public space of each survey object, multiple survey points were selected, according to the different underlying surfaces and the relative distances from the water. In order to facilitate the comparison of different surrounding environments, the current situation of the research objects with the four bodies of water is described in Table 1.

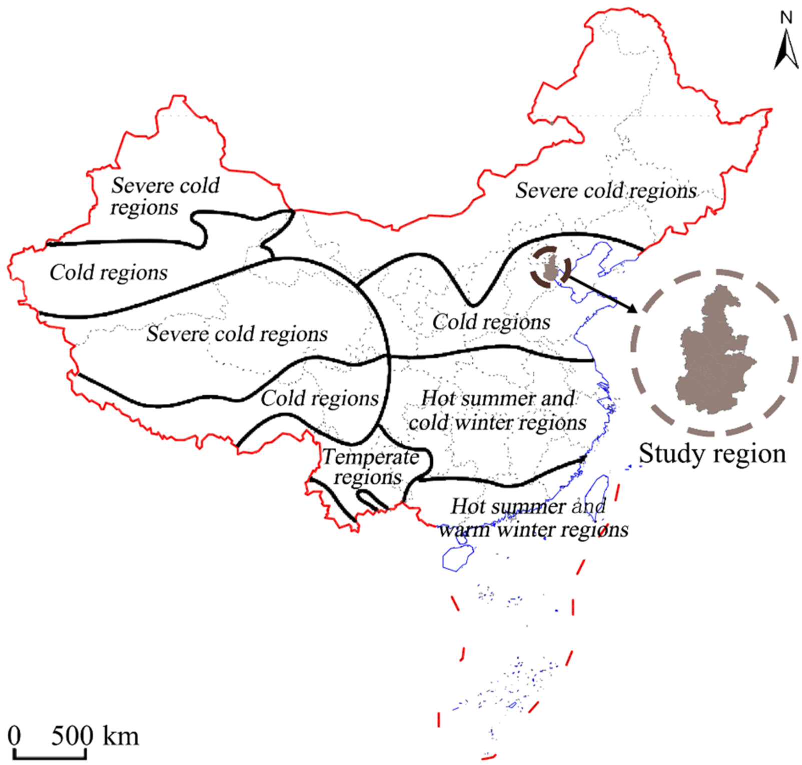

Figure 1. The location of the city and climate zoning.

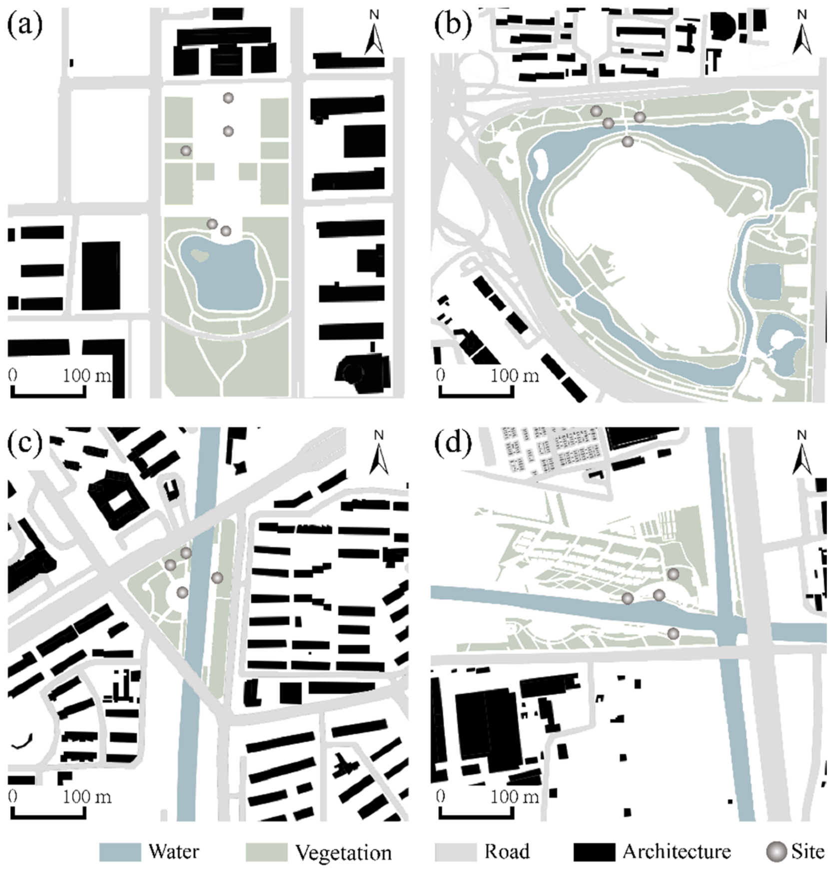

Figure 2. Distribution of field test sites: (**a**) site 1—circular lake; (**b**) site 2—annular lake; (**c**) site 3—a river of north–south orientation; (**d**) site 4—a river of east–west orientation.

Table 1. Environmental description of the measuring site.

Measuring Site	Characteristics of Water Body	Characteristics of Riverbed	Main Activities
Site 1	Circular Lake	Cement Material	Rest and Activity
Site 2	Annular Lake	Natural soil and Stone	Rest and Exercise
Site 3	River of North–South Orientation	Natural soil and Stone	Exercise and Pastime
Site 4	River of East–West Orientation	Cement Material	Rest and Talk

2.2. Methods

2.2.1. Measurement

In this work, a field questionnaire survey, low-altitude infrared remote sensing, and field survey data measurement methods were used to explore those factors conducive to an improvement of the thermal environment in the public space around the urban water in summer in cold regions, and to understand the characteristics of the impact of water on the local geothermal environment. In this study, the 3, 5, 7, 8, 10, and 13 July, in summer when the weather was sunny, were selected as the survey days. A questionnaire survey and field instrument measurements were conducted in the public space around the water body of the circular lake, annular lake, a river of north–south orientation, and a river of east–west orientation, respectively. The measuring time of the instrument was from 8 a.m. to 7 p.m. Due to an error in setting the time of the instrument every day, the time period for data recording varied from day to day, but the data recording was always between 9 a.m. and 6 p.m. The low-altitude infrared remote sensing measurement was mainly conducted in the waterfront space around the water body of the circular lake.

The on-the-spot questionnaire survey is helpful to obtain the most intuitive and direct opinions regarding the investigated objects and to encourage researchers to establish perceptual knowledge of the studied objects. However, inevitably, there will be some drawbacks, such as strong subjectivity. The questionnaire was divided into three parts: (1) basic information, including age and gender; (2) thermal comfort perception, including thermal feeling, thermal comfort, and satisfaction voting, as well as perceptions of sunshine and wind speed; (3) characteristics of behavior and activity, including clothing and activity states. Thermal-sense voting (TSV) used a 7-point scale, namely, very cold, cold, cool, moderate, warm, hot, and very hot, with values of −3, −2, −1, 0, 1, 2, and 3, respectively. In order to carry out quantitative analysis based on low-altitude infrared remote sensing and field survey data measurement, an instrument from WBGT (testoAG Inc., Germany), the tripod of an integrated TR-74Ui-H and TR-73U (T&D Inc., Japan), UAV inspire 1 (DJI Inc., China), equipped with a FLIR TAU2-640 thermal imager and a handheld FLIR T610 thermal imager (FLIR Inc., USA) were used to obtain the measured data for comparative research (Figure 3), which could more scientifically and quantitatively study the thermal comfort of the outdoor waterfront public space. The tripod of the integrated instrument was equipped with a temperature and humidity measuring instrument, TR-74Ui-H, an atmospheric pressure measuring instrument, TR-73U, and a K-type thermocouple, LR9692. The performance parameters of the instruments are shown in Table 2.

The WBGT index was selected as the field measurement evaluation index among the commonly used outdoor thermal comfort evaluation indexes (WBGT, PMV, SET*, PET, UTCI, etc.). The WBGT index is a basic parameter for the comprehensive evaluation of the heat load of human exposure to the working environment, given in centigrade, to evaluate the average heat load of the human body [53]. According to the height of the center of gravity of an upright human body, as specified in the ISO7730 standard, by keeping the probe height of the instrument of WBGT and tripod of instrument integrated at 1.1 m for field survey data collection, the physical environmental parameters around the investigated object could be obtained more accurately [54].

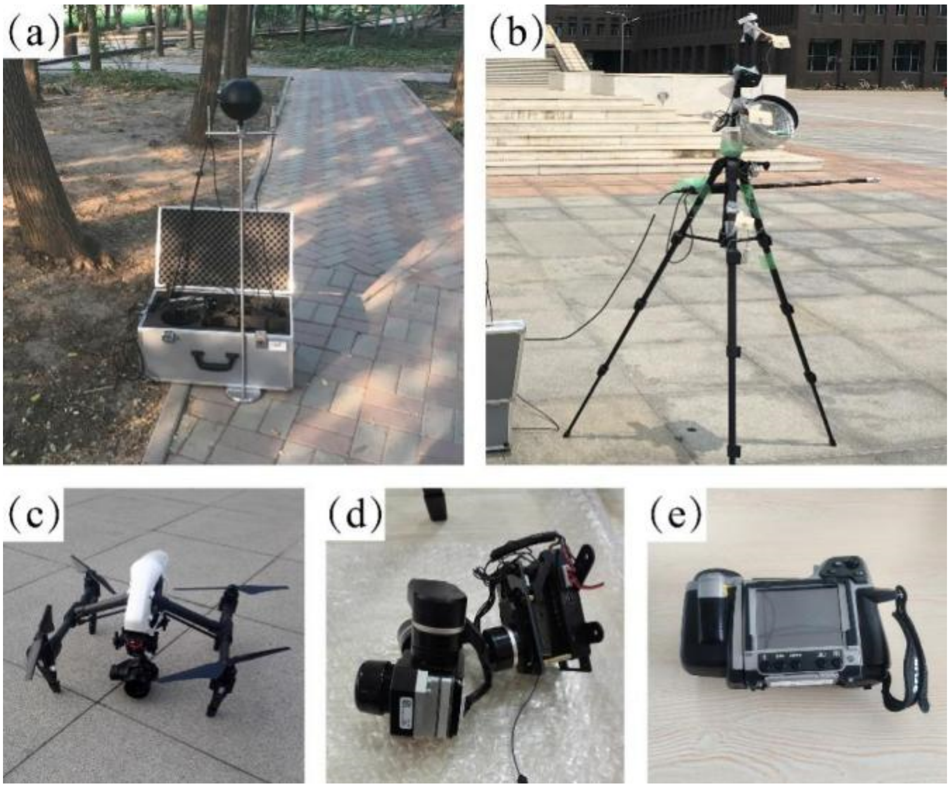

Figure 3. Instrument of research: (**a**) instrument of WBGT; (**b**) tripod of the integrated instrument; (**c**) UAV-Inspire 1; (**d**) PTZ + FLIR TAU2-640 thermal imager; (**e**) FLIR T610 thermal imager.

Table 2. Performance parameters of the main instruments.

Measuring Instrument	Measurement Items	Measurement Accuracy	Resolution
Instrument of WBGT	Temperature Wet Bulb Temperature Relative Humidity Globe Temperature Wind Speed	±0.5 °C ±0.5 °C ±0.5% ±0.5 °C ±3%	0.01 °C 0.01 °C 0.01% 0.01 °C 0.01 m/s
TR-74Ui-H	Temperature Relative Humidity Illumination UV Intensity	±0.3 °C ±5% ±5% ±5%	0.01 °C 0.01% 0.01 lx 0.01 mW/cm^2
TR-73U	Temperature Atmospheric Pressure	±0.3 °C ±1.5 hPa	0.01 °C 0.01 Pa

2.2.2. Simulation

On the basis of the abovementioned environmental intention and physical quantity investigation, through the use of outdoor thermal environment simulation software, it is helpful to simulate different schemes, find their quantitative relationship and purpose, and develop in-depth optimization suggestions on this basis. Currently, ENVI-met, Fluent, CFX, PHOENICS, and Ecotect (Table 3) are widely used worldwide. In this study, ENVI-met was used for the outdoor simulation software to simulate the environment, determine the rules regarding the impact of water on the waterfront space, and formulate an environmental improvement plan. It is an outdoor environment simulation software developed by the German researcher, Michael Bruse [55]. It consists of two parts: one is composed of a three-dimensional modeling module, a soil module, and a boundary module, and the other comprises a nested grid. The software can simulate the outdoor thermal environment by analyzing the thermal characteristics of the building facade materials, the underlying surface, and the fluid. Unlike general steady-state simulation software, it has the advantage of a three-dimensional dynamic simulation, changing over time. The calculation result of the previous time-step is taken as the initial condition of the next step, so it can simulate the process of the external climate environment changing over time more accurately. Its unique grid system can control the simulation accuracy to within 0.1 m and can better simulate the external environment within the microclimate environment.

Table 3. Comparison of simulation software types.

Software	Country	Features	Simulated Types				
			Thermal Environment	Wind Environment	Sunlight Analysis	Pollutant Diffusion	Effect of Plants
ENVI-met	Germany	Commercial numerical simulation software	√	√	×	√	√
Fluent	Britain	Most commonly used commercial CFD general software: Sub-model Airpark is a professional software for HVAC.	√	√	×	√	×
CFX	Britain	Commercial CFD general software	√	√	×	×	×
PHOENICS	Britain	Commercial CFD general software: The physical model is rich, but the grid processing has some limitations.	√	√	×	√	√
Ecotect	America	Commercial CFD general software	√	√	√	×	×

Based on the information provided by field measurement and the questionnaire-based survey, a hypothetical numerical study was carried out to obtain more reliable quantitative results through the ENVI-met model, v4.3. According to the field survey, the number of questionnaires collected by the rivers near site 3 (Figure 4) was very small, and there were not many people who were active there. To increase the residents' desire to go to the waterfront space near site 3 for outdoor activities and improve the comfort of the thermal environment of such a region, this site was selected as the objective for simulation and improvement. Numerical simulations were conducted on 8 July. The simulated background meteorological data were obtained through hourly field measurement, which was utilized for the simple forcing settings in ENVI-met. The microscale model domain had a surface area of 57,600.0 m^2 (240.0 m $\times$ 240.0 m), divided into 60 $\times$ 60 square grids with 4.0 m resolution on the horizontal surface. There were 30 vertical telescoping grids with an initial resolution of 4.0 m. The main study region was the waterfront hard surface, and the influence of water on the environment was explored. Geometric information and green and blue space dimensions were derived from the relevant Google Earth™ satellite images and field investigation. In this microscale model, water and greenery were given a simplified treatment. We selected the default 4.5-m-deep waterbody of the software, which was appropriate to the actual situation. Greenery included grass (0.3 m height), as was similar to reality. The relevant simulation parameters are shown in Tables 4 and 5.

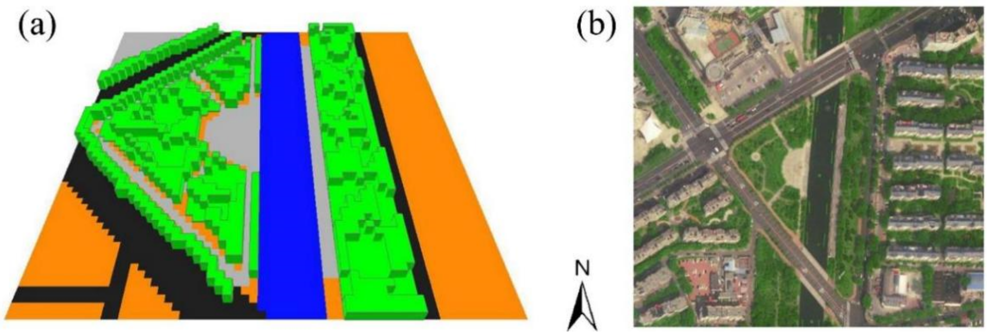

Figure 4. (**a**) Simulation model of site 3; (**b**) satellite remote sensing of site 3.

Table 4. Preset values of the simulation parameters of site 3.

Type of Vertical Grid	Resolution of Grid	Number of Grids	Number of Nested Grids	Type of Nested Grid Soil
Equidistant Grid	$d_x = 4$ $d_y = 4$ $d_z = 4$	60 × 60 × 30	3	Fertile Soil

Table 5. Analog data settings of site 3.

Duration of Simulation	Maximum and Minimum of Temp.	Initial Relative Humidity	Cloudiness	Type of LEC	Initial Wind Speed	Direction of Wind
12 h	36 °C/28 °C	7%	Clear Sunny	Open Form of Temperature and Humidity/Closed Form of Turbulence	2 m/s	Southeast (155°)

The software also cannot calculate the influence of a gentle and vertical riverbank, so we chose to study the width of the water, a platform anchored to the riverbed in the water, and the layout of the green space. In order to study the effect of the water width on the surrounding environment, the width of the water in Figure 4 was taken from 40 m to 100 m in steps of 10 m. By studying the limit value of the water improvement effect, the most economical river width could be calculated. During the modification of the square, the platform went far into the center of the waterbody to explore the environmental impact of the water on the riverbank. The simulation objects were the current situation of the square (Figure 5a), simulation 1 of the square (Figure 5b), and simulation 2 of the square (Figure 5c). In terms of including auxiliary underlying surfaces to improve the cooling effect of the water, such as greenery (trees, shrubs, and lawns), we mainly studied the cooling effect of lawns in conjunction with water. According to the previous research, the combined effect of trees, shrubs, and lawns enhanced the cooling effect significantly, and green lawns without vegetation shade were found to be least effective compared to green lawns with trees and shrubs for the mitigation of UHI [56,57]. However, this paper mainly studied the cooling effect of water on the waterfront space, and the cooling effect of trees and shrubs to improve the waterfront environment in the shade was much more obvious than that of water. The cooling effect of the water was almost negligible under such conditions, which was not consistent with our original intention of revealing the cooling effect of water. Meanwhile, trees and shrubs could work together with water to cause synergistic cooling effects (SCEs), which this study did not include, and SCEs were beyond the scope of water itself affecting the thermal environment of waterfront space [58]. Furthermore, the cooling effect of trees and shrubs would be mainly affected by greenery height, greenery planting density, and the greenery species themselves. Therefore, the lawn was the main research object to improve the water's UHI mitigation, instead of trees or shrubs in this section. Because the layout of green lawns should take into account the residents' activity space, with different widths between lawns, lawn spacings of 4 m, 12 m and 24 m were chosen and discussed (Figure 6).

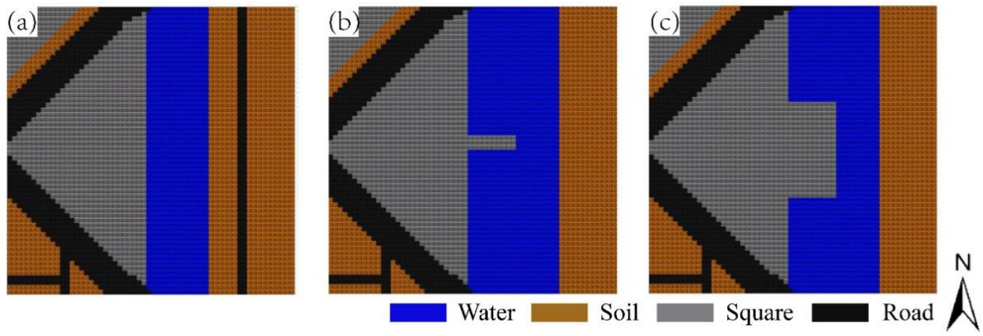

Figure 5. (**a**) Original site layout of the square; (**b**) simulation 1 of the square; (**c**) simulation 2 of the square.

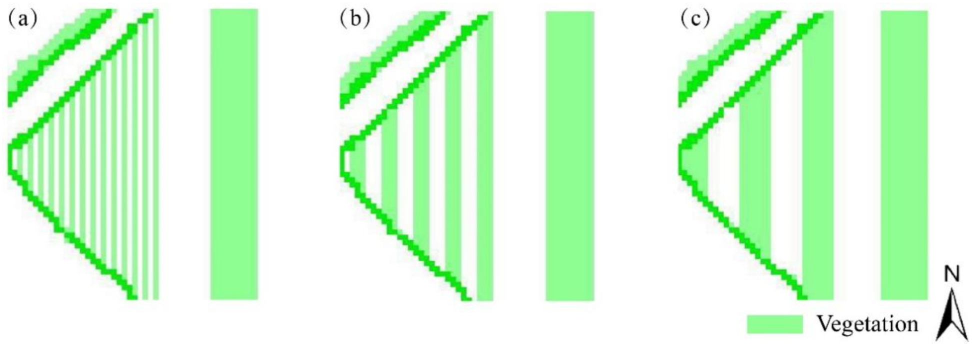

Figure 6. (**a**) Simulation 1 of the green space—4 m pitch; (**b**) simulation 2 of the green space—12 m pitch; (**c**) simulation 3 of the green space—24 m pitch.

3. Results and Discussion

3.1. Assessment of Waterfront Environment

3.1.1. Subjective Assessment

In this work, 141 valid questionnaires were obtained from people aged from 25 to 80 years old, comprising 87 males and 54 females. Among them, 27 questionnaires were collected from site 1, 49 from site 2, 11 from site 3, and 54 from site 4. The number of respondents in site 3 was the lowest, and 11 valid questionnaires were received. Those who came to the activity in the morning had no data for other time periods. Since most of the students carried out activities in the public space near the central lake of site 1, their class time was regular, and their leisure time by the water was limited in the daytime, so they were not included in the statistics. Included in the statistics were the public activity spaces near site 2 and site 4, with 73 and 57 person-times, respectively. The surrounding construction environment of water was relatively attractive, with open seats, dense tree plantings, and activity equipment, which were suitable for residents living nearby to carry out activities. The subjective evaluation was concluded as follows:

1. The comfort level of the human body is affected by environmental factors, physiological factors, physical cooling, and psychological factors.
2. The degree of human comfort in a waterfront area was significantly affected by the air humidity. The higher the air humidity, the more comfortable people felt.

3. The comfort degree of the human body in a waterfront area was affected by the wind speed, and the optimum wind speed was closely related to the comfort degree of the human body. When the water body was affected by cool winds, the comfort evaluation was significantly higher.
4. The degree of comfort in a waterfront area was restricted by the illumination, the amount of exercise, drinking water, the use of physical cooling and the degree of psychological pleasure—the more effective the physical cooling, the higher the degree of comfort.

3.1.2. Objective Assessment

Taking site 1 (Figure 7) as the evaluation object of the infrared thermal images, the conditions of the outdoor thermal environment of the target site were evaluated by two kinds of infrared thermal image-carrying modes. By setting the radiation coefficient appropriately, the temperature difference between the objects could be reflected more accurately. In this study, infrared thermal images were analyzed using ViewSeri v2.1, which is software used for analyzing and viewing FLIR digital infrared images on the computer. Here, the software was used to switch color between various palettes of infrared images and display the surface temperature at any observed site in the infrared image, as well as the maximum surface temperature in any region. Therefore, the objective assessment of the waterfront's thermal environment regarding the surface temperature was conducted via color differences from infrared thermal images (qualitative evaluation) and the software display side (quantitative evaluation). From this point of view, the application of infrared imaging to test the outdoor thermal environment offers a certain reliability.

Through the study of handheld infrared thermography (Figure 8a), we found that the surface temperature of the water rose slowly. The surface temperature of the water was low at 9 a.m. and rose to about 25.50 °C. The surface temperature rose to 28.40 °C at 1 p.m. and again to 29.10 °C at 7 p.m. Finally, the surface temperature reached a peak at a set point between 1 p.m. and 7 p.m. After the peak, it fell back to the surface temperature, close to noon. The surface temperature of the water was higher in the evening, which had a set heat storage capacity. This would affect the surface temperature of the reservoir bank, especially at 7 p.m., when the surface temperature difference among the water body, the water bank, and the water bank was minor. The degree by which the water improved the surrounding environment was greatly lessened at night. In summary, it was found that the surface temperature difference between the water body and the surrounding environment was larger at noon and smaller in the evening, indicating that the influence was more obvious at noon and weaker in the evening.

Through the use of UAV infrared thermography (Figure 8b), we found that the influence of water on the surrounding square is minor. Only the surface temperature of the adjacent water within 8 m could be reduced significantly, and the average surface temperature above 16 m was almost the same as that in the square. In the daytime, the surface temperature difference between the water and the environment was large, and the surface temperature of the body of water was low. Through different emissivity calculations, it could be established that the surface temperature of the water body was 5.98 °C lower than that of the surrounding parkland, and 12.28 °C lower than that of the hard paving beside the water. There was a large surface temperature difference between the water body and the surrounding environment, which might affect the surface temperature of the surrounding environment. In the evening, as the water absorbed heat, its surface temperature rose. At the same time, the heat release of the hard pavement was rapid, and its surface temperature dropped. The temperature of the water surface was 30 °C, that of the hard pavement near the water surface was 30.28 °C, and that of the hard pavement far away from it was 32.02 °C. The water surface no longer had an increasing influence on the surrounding environment, so its influence was far less than that in the daytime.

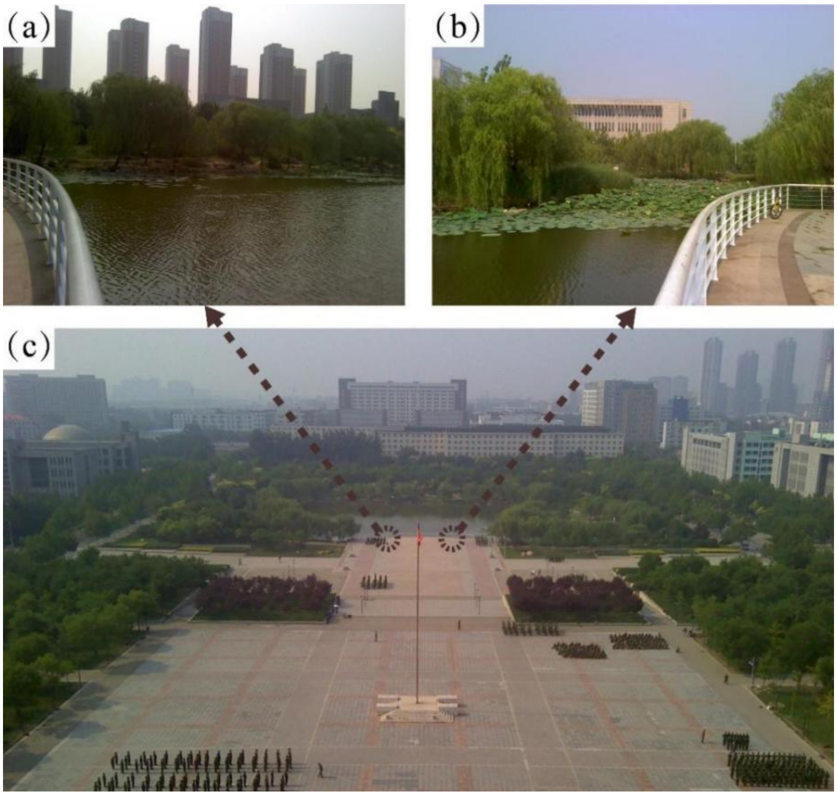

Figure 7. Location of infrared thermography assessment: (**a**) left space; (**b**) right space; (**c**) waterfront plaza.

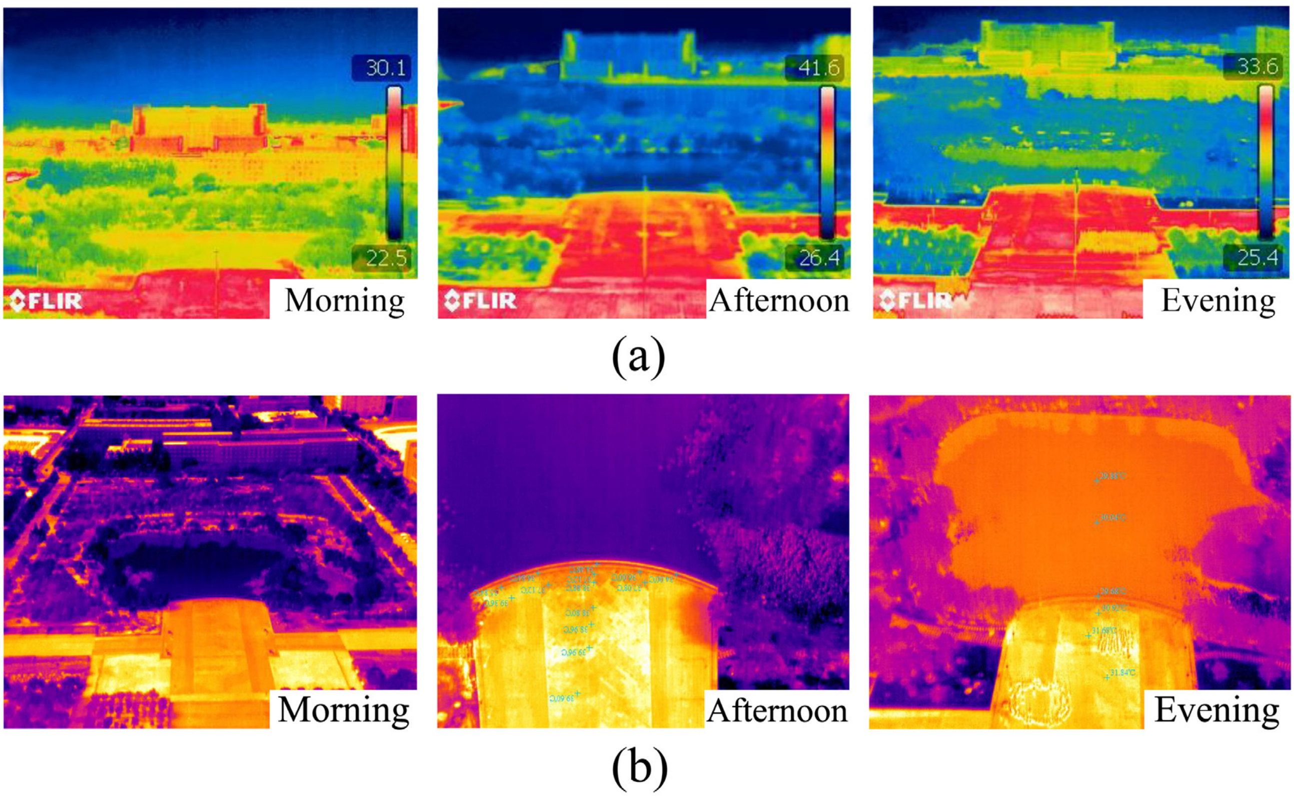

Figure 8. Images of the waterfront plaza using infrared thermography: (**a**) handheld infrared thermography; (**b**) UAV infrared thermography.

3.2. Analysis of Measured Data

3.2.1. Influence of Water on Different Underlying Surfaces

The comparison of measurement sites followed the principle of controlling variables, and the principle of controlling a single variable ensured that the comparison was more rigorous. Due to the limited instruments, only one test point could be tested every day. Every comparison item was the same day's test point comparison. The distance between the two test points was within a certain range, which ensured that factors other than the measurement factors were the same. Theeuwes et al. [59] found that the larger the area of water was, the greater its effect on the urban thermal environment. In this work, to establish the difference in human thermal comfort (WBGT evaluation) between the locations adjacent to the water and waterfront spaces far away from the water, a planar water model with a large area at site 1 was taken as an example, using various underlying surfaces. Meanwhile, to analyze the performance of UHI mitigation (air-temperature comparison) by bodies of water in various formats (planar and linear water), the different underlying surfaces around the planar water of site 1, and the linear water of site 4 were selected for this study.

Figure 9a–c shows the WBGT value and temperature comparison diagrams of the waterfront square and the square farthest away from the water, where the underlying surface was hard pavement. By comparison, it could be found that the average WBGT value of the square farthest from the water was 30.21 °C, and the average WBGT value of the waterfront square was 30.00 °C, which was 0.21 °C lower than that farthest away from the water. The change in the WBGT value farthest away from the water was relatively minor, and the change in the WBGT value in the waterfront square was more profound. Additionally, the WBGT index around the water fluctuated greatly with high frequency. The improvement of the thermal environment of the waterfront square was obvious, which could reduce the average temperature by about 1.00 °C in the presence of the planar water. In addition, the cooling effect of the linear water for the hard pavement was about 0.90 °C, lower than 1.00 °C. The reason for this was that the area of the linear water in the waterfront plaza at this location was much smaller than that of the planar water. On the basis of the above-mentioned conclusions, we could explain the characteristics of the fluctuation frequency and amplitude of the impact of water on the environment, and proved that the waterfront environment was more suitable for all activities, regardless of waterbody formats.

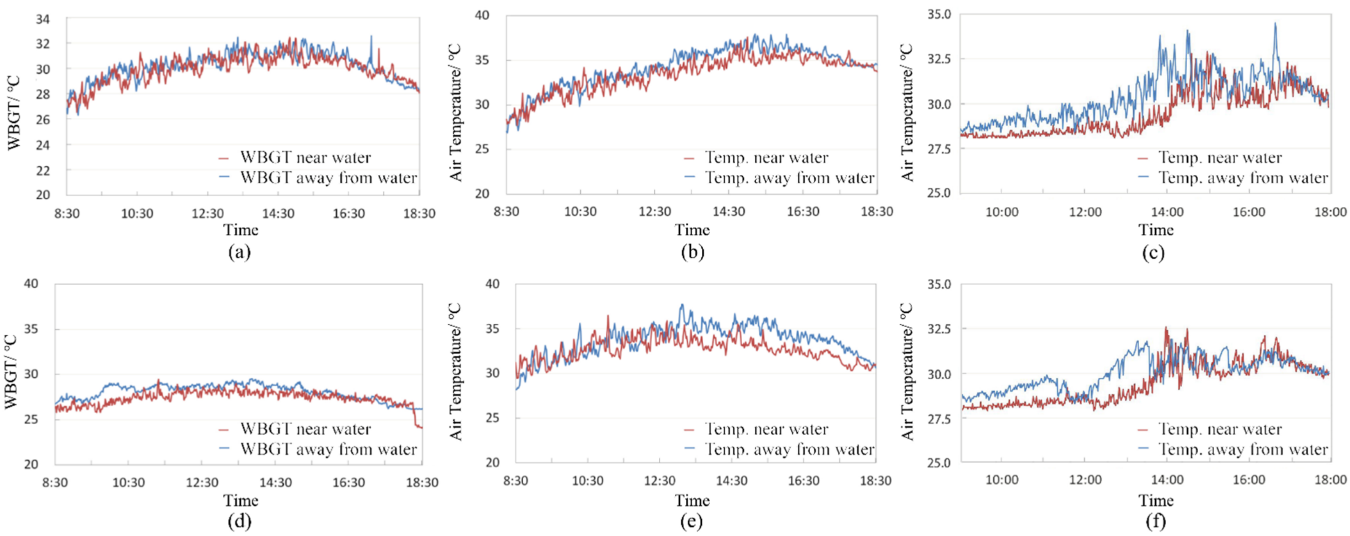

Figure 9. (**a**) WBGT comparison of hard pavements; (**b**) temperature comparison of hard pavements around planar water; (**c**) temperature comparison of hard pavements around linear water; (**d**) WBGT comparison of green spaces; (**e**) temperature comparison of green spaces around planar water; (**f**) temperature comparison of green spaces around linear water.

Figure 9d–f shows the WBGT values and temperature comparison diagrams of the forest and grass surfaces of the spaces near water and the space farthest away from water. It can be seen that the environmental values around the water fluctuated significantly, indicating the periodicity of the water's impact on the environment. The environment farthest away from the water was warming up, while the waterfront space had not yet begun to warm up. The environment was cooling, and yet the waterfront space was not cooling. Waterfront space had a delayed effect on environmental changes. In the presence of green spaces, the waterfront space was more comfortable before 5 p.m. than the area away from the water, and that was more comfortable after 5 p.m. The temperature of the waterfront space around planar water was higher than that of the space farthest away from water before 10:30 a.m. but was lower than that after 10:30 a.m. The temperature of the waterfront space around the linear water was significantly lower than that of the space away from the water before 2 p.m., while there was almost no difference after 2 p.m. Different area and width of two water formats, as well as shading modes for tall deciduous trees, made certain distinctions. However, under the condition where there were two water formats, the general temperature of the waterfront space next to the green space was always lower than that of the square next to the green space. The temperature difference between morning and evening was minor, and the change was stable. By comparing the thermal environment of waterfront space with or without green spaces, it was found that the thermal environment with a green space was more comfortable than that without a green space.

3.2.2. Thermal Comfort Analysis of the Riverbank

By comparing the data from the east and west banks of site 3 (Figure 10a), it was found that the temperature trend of the east and west banks was basically the same, the peak temperature of the curve on both sides was at about 4:30 p.m. and the peak temperature of WBGT was about 3 p.m. However, the index values of the west bank were obviously higher than those of the east bank. From the WBGT value, we could see that the thermal environment on the east bank was more suitable for people who wished to rest. The temperature change span of the east bank was small, and the fluctuation shown by the broken line was drastic and obvious. Compared with the west bank, the average temperature of the east bank was 2.19 °C lower than that of the west bank. From Figure 10a, we could see that the WBGT index of the east bank was much lower than that of the west bank. The WBGT value and temperature of the west bank were almost the same; finally, they came together at almost the same time. In addition to the temperature, other environmental factors did not improve the reported discomfort caused by the temperature. In addition, the bright sunlight in the afternoon on the west bank aggravated the subjects' discomfort. Therefore, according to the climate of Tianjin, it was more appropriate to design a public meeting space on the east bank of the north–south river. By comparing the data of the north–south bank of site 4 (Figure 10b), we could see that the change in the WBGT value on the north bank was relatively minor, while the change in the WBGT value on the south bank was relatively large, the frequency was very high, and the fluctuation was drastic. This showed that the temperature on the south bank was obviously affected by the presence of the water. Compared with the south bank, the average temperature of the north bank was 0.01 °C higher than that of the south bank, and the average WBGT value was 1.23 °C higher. It was found that WBGT values intersected around 11 a.m. Before 11 a.m., the north bank was more comfortable. After 1 p.m., the south bank was more comfortable. From a comparison of the north–south river and the east–west river, the east bank was more comfortable than the west bank all day. The south bank and the north bank changed over time. The north bank was comfortable before 1 p.m., and the south bank was more comfortable after 1 p.m. However, before 11 a.m., the temperature was more comfortable during the day, so the comfortable climate of the south bank warranted further attention.

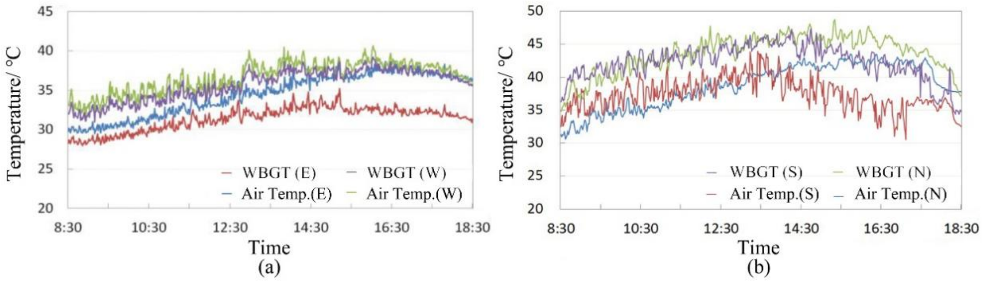

Figure 10. (**a**) Comparison of indexes at site 3; (**b**) comparison of indexes at site 4.

3.2.3. Analysis of Thermal Environment above the Water

Figure 11a,b shows the comparison of the thermal comfort of the area far into the water. The test site was located on the small bridge of site 2. The annular lake had a large area. Through comparisons, it could be found that the temperature, humidity, and WBGT index in the center of the water were relatively attractive, and the temperature was low. There were almost no fluctuations in temperature, humidity, and WBGT. The temperature difference between morning and night was very small. This showed that the temperature on the water surface was in a stable state, and the environment was not changed by the external changes. This also showed that water was a good "buffer", which could decrease the speed of temperature and humidity changes and provide a regulatory function. The average temperature was 36.12 °C, and the average humidity was 50.25%. The relative humidity above the water was high, and the temperature was not very low. However, WBGT showed good comfort and stability. Although the environment on the bridge was attractive, it was not comfortable compared with the shady waterside environment. Through comparison, it can be seen that the temperature, humidity, and WBGT index in the center of the water were very low, and the temperature was low, indicating that the deeper the water was, the more obvious the improvement effect.

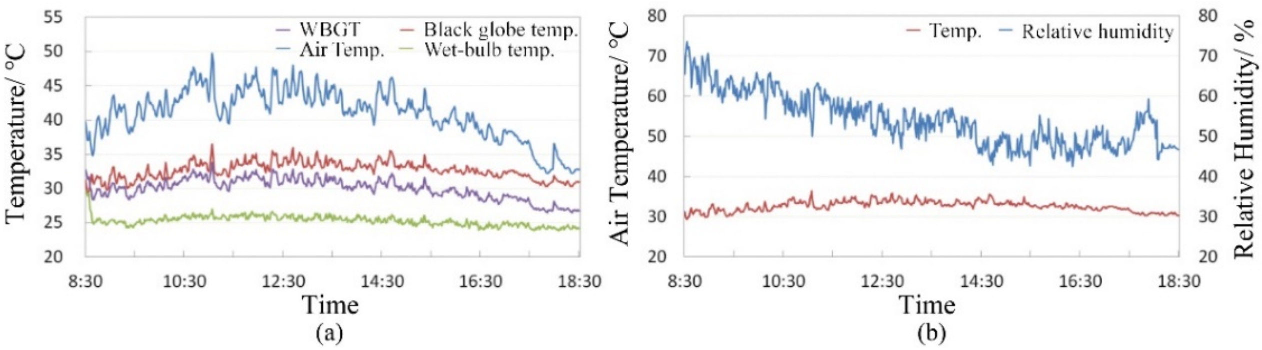

Figure 11. (**a**) WBGT of site 2; (**b**) temperature and humidity of site 2.

3.3. *Analysis of Simulation*

3.3.1. Verification of Model Accuracy

ENVI-met was used to simulate the thermal environment of the waterfront space. After checks, the simulation results for cold regions were obtained. The simulation data would be compared with the measured data. To account for the complicated effects of underlying surface conditions, the simulated air temperature and relative humidity of the waterfront's hard surface were extracted for comparison with the measured data at a similar site (Figure 12). It can be seen from Figure 12 that the change trend and magnitude of measured and simulated values were the same. The ENVI-met estimation outputs for air temperature and relative humidity were in good agreement with the measured values. This study employed Root Mean Square Error (RMSE) and Mean Absolute Percentage Error (MAPE) to evaluate the validity of the simulating model. Lower values for RMSE and MAPE indicate better model performance, and an acceptable performance requires an

RMSE with an air temperature of less than 1.31 °C and a MAPE of relative humidity of less than 5.00% [60,61]. The equations for RMSE and MAPE are shown below:

$$RMSE = \sqrt{\frac{1}{r}\sum_{i=1}^{r}\left(y_i' - y_i\right)^2} \tag{1}$$

$$MAPE = \frac{1}{r}\sum_{i=1}^{r}\frac{\left|y_i' - y_i\right|}{y_i} \times 100\% \tag{2}$$

where r is the total number of groups, y_i' is the simulated value of the ith parameter, and y_i is the measured value of the ith parameter.

The ENVI-met model has been verified in many regions [62,63]. Overall, RMSE and MAPE have shown consistency between the simulated data and the observed results in this study, with RMSE and MAPE of 1.13 °C and 4.32%, respectively. Therefore, the ENVI-met model was verified by comparing the measured and simulated data, and RSME and MAPE were used to validate the accuracy.

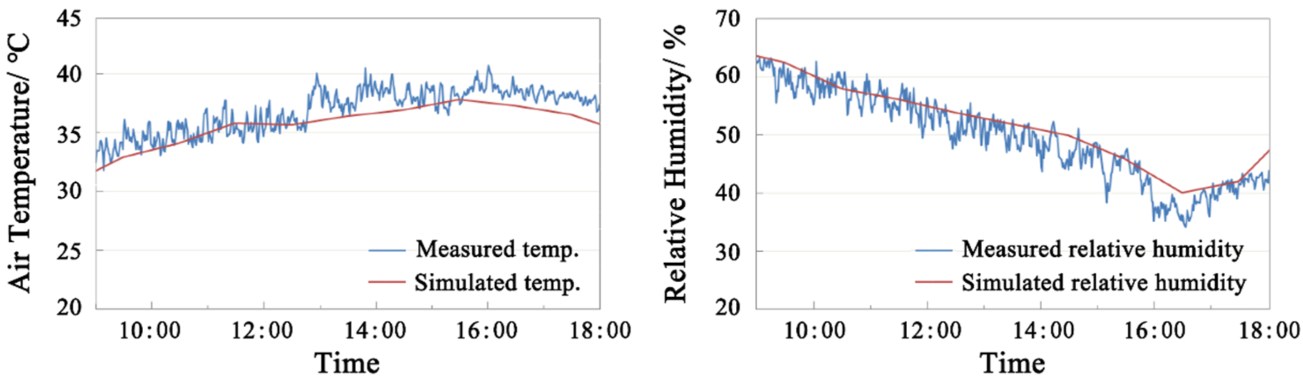

(**a**) (**b**)

Figure 12. Waterfront temperature and relative humidity of measurement and simulation: (**a**) air temperature; (**b**) relative humidity.

3.3.2. Water Width

From Figure 13, it is clear that the greater the width was of the body of water within 70 m from the square of site 4 to the waterfront, the more obvious was the improvement effect on the surrounding waterfront space. There were no obvious advantages and disadvantages for the line chart with waterbody widths of 70 m, 80 m, 90 m, and 100 m. The effect of a body of water of between 70 m and 80 m on environmental improvement was similar, reaching a balance. However, the opposite effect was observed in the rivers of 90 m and 100 m in width. The temperature in the area farthest away from the water was higher, and the temperature drop in the area near the water was more obvious. This showed that the influence of a river with a width of more than 70 m was similar to that of a river with a width of 70 m. The river with a width of 70 m was the most suitable for the square with an area of 100 m around the water bank, and its influence was the most significant. Therefore, it was concluded that the design including a river width of between 70 m and 80 m had the best effect on improving the thermal environment of the waterfront space.

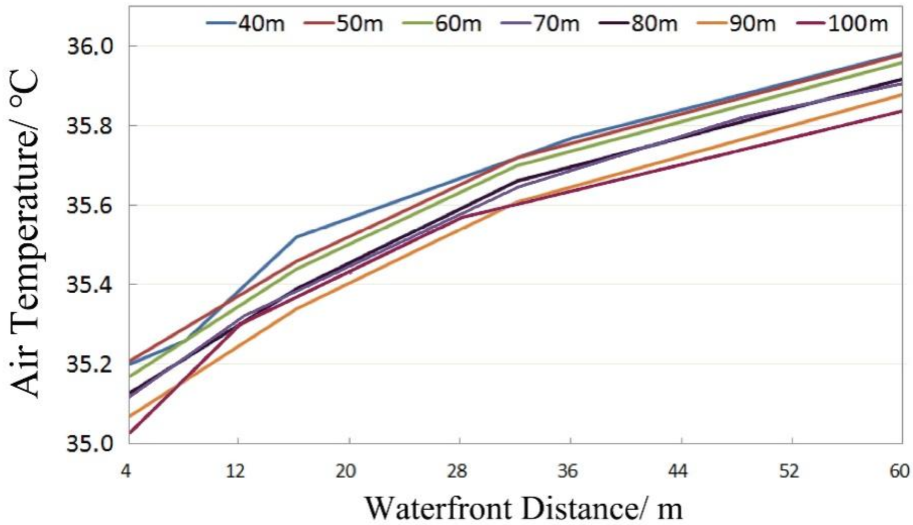

Figure 13. The temperature at different river widths.

3.3.3. Platform Located in the Water

After the simulation (Figure 14), it was found that the change in location environment was obvious in the deep-water square, and there was no obvious change in the original square area. The temperature distribution of the original square showed a slight change, breaking the original triangle-like fan-shaped change pattern. From the temperature curve, we can infer that should the area deep into the water increase, the curve would be very different from the original, so the simulation 2 of the square was carried out. Generally speaking, when increasing the area of the square, the improved area also increased, so that if the square could be moved deep into the waterbody, this would improve the impact area of the water on the surrounding environment. The simulation results showed that the square further into the water area was improved, but there was no change in the regional temperature distribution further into the water. According to the simulation results, by increasing the side length of the windward riverbed and calculating the improved width, if the improved width completely covered the whole square, then the improvement of the water environment was more economical. This is to say that when the area of the square deep into the water was the same as that of the water, which might improve the environment, the square area was the most economical.

3.3.4. Waterfront Vegetation

By comparing the measured air temperatures of the waterfront lawns and the waterfront hard surface at the measurement site (Figure 15), it can be seen that although the difference between the temperature of the waterfront lawn and the waterfront hard surfaces before 12:30 p.m. was not significant, the temperature of the waterfront lawn after 12:30 p.m. was obviously lower than that of the waterfront's hard surfaces. This could support the assertion that the UHI mitigation effect of waterfront lawns was greater than that of the waterfront hard surfaces in this study. Therefore, the numerical simulation of lawns to improve the water's cooling effect was conducted, as follows. Through the simulation scheme, we found that the more concentrated the grass area, the better the cooling effect. Therefore, planting a wider grass belt at the junction of the river and riverbank had a better impact on the thermal environment. The lawn areas of the simulations 1–3 of the green space were similar. When comparing them (Figure 16), the cooling effect of the simulation 2 of the green space was better, and the influence area was the largest. Although the simulation 3 of the green space increased the width of the grassed area, it did not have a better effect. When the density of the lawn design was at a certain scale, the improvement to the environment was more obvious. In the layout of site 4, the width of the lawn was designed to be 12 m, and the width of the granite area was designed to be 12 m.

It could be concluded that the larger the area of water that was provided for environmental improvement, the more obvious the effect.

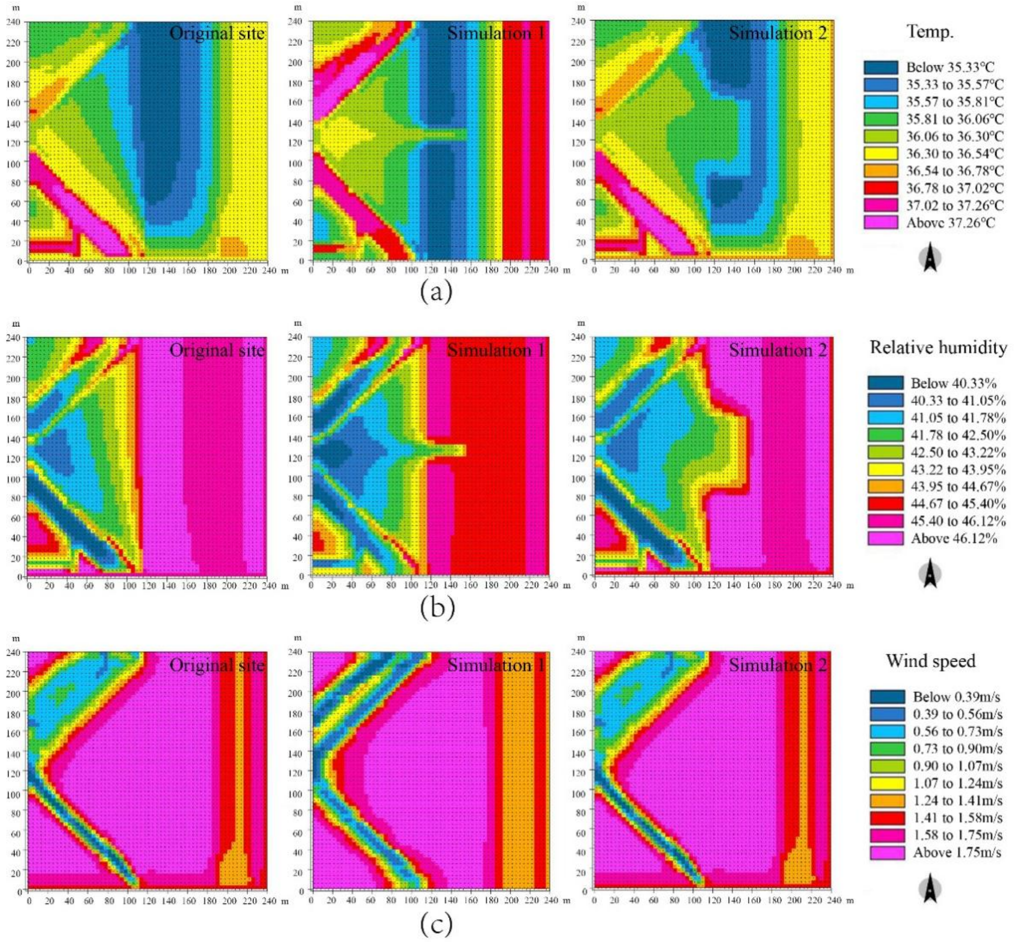

Figure 14. (**a**) Comparison of temperature; (**b**) comparison of relative humidity; (**c**) comparison of wind speed.

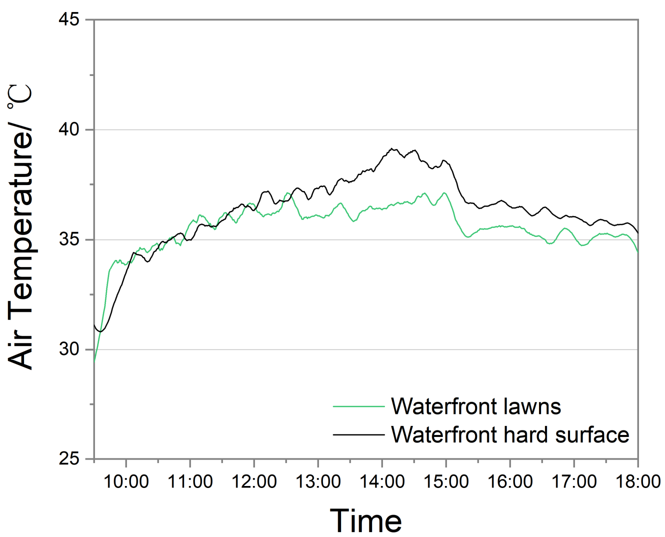

Figure 15. Air temperature comparison of waterfront lawns and hard surfaces.

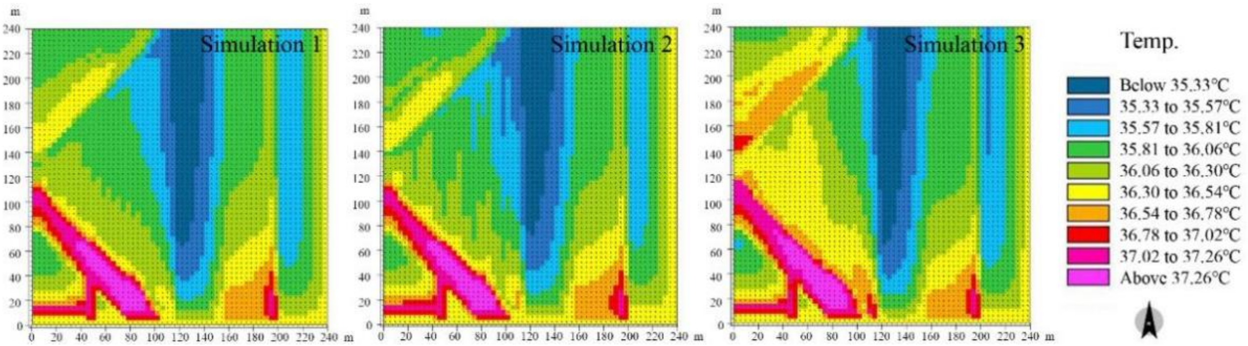

Figure 16. Comparison of temperature in various simulations of the green space.

3.3.5. Optimization Design

Through the induction and summary of the above simulation analysis, the waterfront space near site 3 was optimized (Figure 17). The optimal scheme improved 80% of the temperature comfort of the area on the square. The distribution of the riverbank was S-shaped, which could make the riverbank perpendicular to the wind direction to the greatest extent and most improve the auxiliary environment of the lawn. The principle of the design was to ensure that the square area remained unchanged; the riverbank was parallel to the wind direction to the greatest extent and the lawn spacing was at the most optimal value of 12 m. The distance for pedestrians to walk was set at the lawn area, to obtain the corresponding temperature, humidity, and wind speed changes. Comparing the simulation results (Figure 18) with the original environment scheme of site 3, it could be seen that the improved area increased obviously after the amendment of the scheme. When the original square was not planted with trees, the water improvement area accounted for 34% of the total area, and the improved area after adjustment was 90.9%. The area with the best improvement showed a decrease of 1.26 °C, and the improvement effect was desirable.

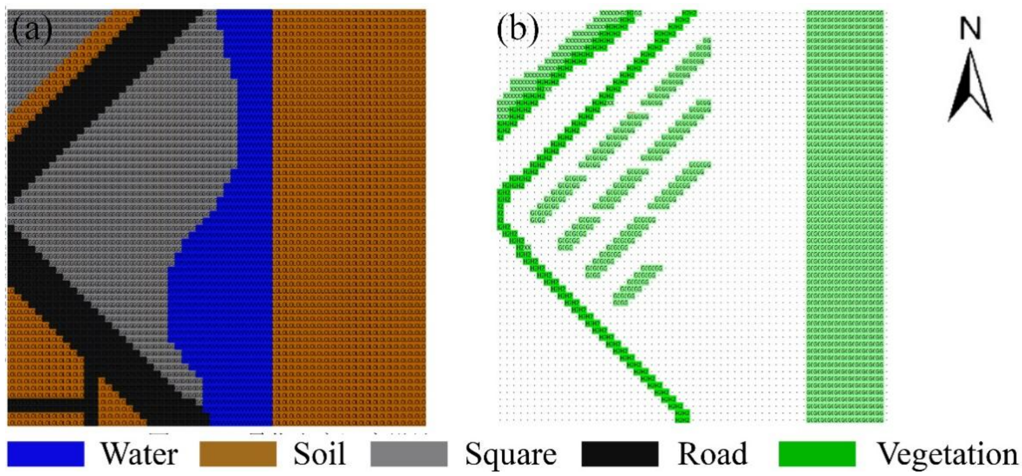

Figure 17. (**a**) Design of riverbed; (**b**) design of green land.

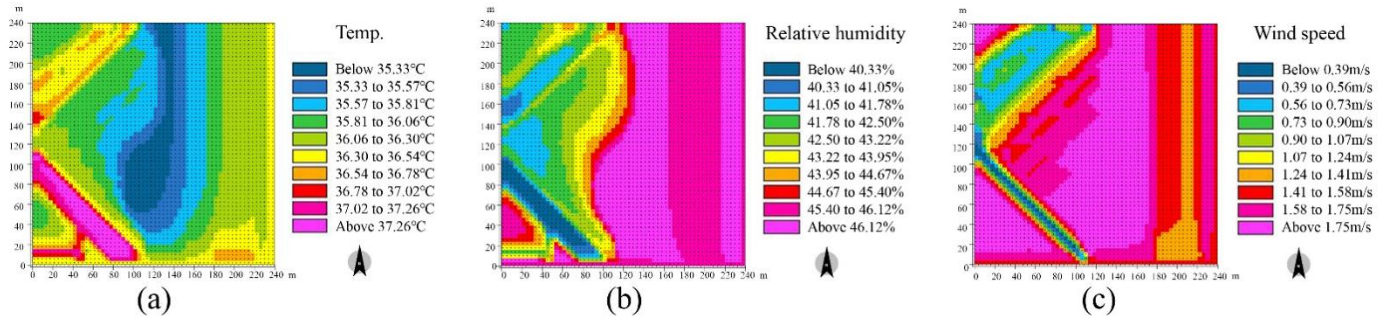

Figure 18. (**a**) Temperature distribution; (**b**) relative humidity distribution; (**c**) wind speed distribution.

3.4. Differences from Previous Studies

The methods of field measurement and numerical simulation were easy to conduct, and other methods, such as low-altitude remote sensing and the questionnaire survey, made it difficult to establish an interrelated analysis of the water's UHI mitigation. Therefore, previous research mainly emphasized a single method, such as field measurement and numerical simulation, lacking a comprehensive analysis and evaluation [38,59]. This study conducted a thorough evaluation and frame construction based on multiple methods, making it easier to analyze the water's cooling effect and thermal evaluation standard. Finally, the contribution of water toward UHI mitigation was discussed in terms of the cooling effect, underlying surface types, riverbank orientation, the thermal environment above water, and water width. In addition, urban greenery (green lawn spacing) and geometrical forms (S-shaped riverbank) were reported to improve the water's cooling effect.

The cooling effect of water arises from a very complex and comprehensive ecological process. Many scholars have explored the cooling effect of water. However, Wang et al. [64] mainly focused on the effect of large-scale water and greenery, while this study investigated the cold regions in China, where small- and medium-sized water bodies were common, as the objective by which to explore the cooling effect of water. Different climate regions could affect the study results significantly [56–58]. There was a relative lack of research on the UHI mitigation effect of water in China's cold regions, compared with previous studies. Previous studies were excessively focused on the waterbody effect via temperature contrasts, but this study used a comprehensive comfort index to evaluate the cooling effect of water on the thermal environment [44]. This was because previous studies were based around the research framework of UHI, which emphasizes temperature contrasts. Hathway et al. [26] reported that a 22-m-wide river could cool the waterfront space by 1.5–2.0 °C; however, this study not only revealed the cooling effect of water but also explored the law that green lawns and riverbank shape improved the cooling effect intensity of water. This study tallies with the constraint factors of planning and design and can provide guidance based on specific layout conditions for practical construction.

4. Conclusions

Based on the field investigation of the outdoor thermal environment of four typical urban water and surrounding spaces in Tianjin, different optimization schemes for outdoor waterfront space were simulated. The contribution toward UHI mitigation by means of water was reported, as follows. The surface temperature difference between the water body and the surrounding environment was greater in the daytime and less in the nighttime. The waterfront's underlying surface was more enjoyable for activities than the underlying surface farthest from the water. The east and south riverbanks' thermal comfort should be emphasized. The influence of water was affected by the distance between the measured site and the water center; the closer to the water center the measurement site was, the more obvious the cooling effect. The most economical water width should be designed as 70–80 m. In addition, when the lawn spacing of the waterfront space was 12 m and the water shore bank was S-shaped, these changes could improve the cooling effect of water greatly.

The improvement effect of the water on the surrounding thermal environment was very significant. This study clarified the improvement rules and the quantitative relationship with water for the surrounding thermal environment. It is suggested that the planning and layout of waterfront space should focus on the water width, the main human activity space's layout, the spacing of green lawns, and the water shore geometry form, to improve the intensity of the cooling effect of water. It is not necessarily the case that a wider body of water is better. The distribution of the main human activity space should pay attention to its distance from the center point of the body of water, and the orientation of the water shore. The arrangement of grassed areas needs to adopt the rationalized spacing mentioned in this study, according to the actual demands of people using the activity space. The shape of the water's shore should also be kept close to the center of the water body, such as the S-shaped riverbank revealed in this study.

This study can provide great theoretical support for the design of waterfront spaces, can create more appealing outdoor areas, and increase people's desire for outdoor activities. Additionally, this paper works as a reference for studying outdoor thermal environments in China's cold regions, especially regarding the cooling effect of water. It proposes a plan to improve the waterfront environment. Moreover, the findings will help to further mitigate the UHI effect and improve thermal comfort for urban residents.

In terms of weaknesses, this study's choice of green spatial patterns, in which we mainly focused on green lawns, could have been better diversified, and further in-depth studies on the roles of the relevant factors need to be performed in China's cold regions, such as the types of vegetation, the heights of buildings, and wind speed. Moreover, seasonal variations in the cooling effect of water were not analyzed, and a comparison of the various climatic regions and seasonal data should also be utilized in the future to make the UHI mitigation analysis more comprehensive. In general, this study yielded a comprehensive comparative analysis of all factors in a built-up waterfront area.

Author Contributions: Conceptualization, F.F. and Y.W.; methodology, F.F., Y.W. and X.J.; software, F.F. and X.J.; validation, F.F., Y.W. and X.J.; formal analysis, X.J.; investigation, Y.W. and X.J.; resources, F.F. and Y.W.; data curation, F.F. and X.J.; writing—original draft preparation, F.F.; writing—review and editing, F.F.; visualization, F.F.; supervision, Y.W.; project administration, Y.W.; funding acquisition, Y.W. All authors have read and agreed to the published version of the manuscript.

Funding: This research was funded by The National Natural Science Foundation of China, grant number 51678386, and The Opening Fund of State Key Laboratory of Green Building in Western China, grant number LSKF202201.

Institutional Review Board Statement: Not applicable.

Informed Consent Statement: Not applicable.

Data Availability Statement: Data available on request due to restrictions e.g., privacy or ethical.

Acknowledgments: The authors are grateful for the support of The National Natural Science Foundation of China (51678386) and The Opening Fund of State Key Laboratory of Green Building in Western China (LSKF202201).

Conflicts of Interest: The authors declare no conflict of interest.

References

1. Bocquier, P. World Urbanization Prospects: An alternative to the UN model of projection compatible with the mobility tran-sition theory. *Demogr. Res.* **2005**, *12*, 197–236. [CrossRef]
2. Sun, Y.; Gao, C.; Li, J.; Wang, R.; Liu, J. Evaluating urban heat island intensity and its associated determinants of towns and cities continuum in the Yangtze River Delta Urban Agglomerations. *Sustain. Cities Soc.* **2019**, *50*, 101659. [CrossRef]
3. Marando, F.; Salvatori, E.; Sebastiani, A.; Fusaro, L.; Manes, F. Regulating ecosystem services and green infrastructure: Assessment of urban heat island effect mitigation in the municipality of Rome, Italy. *Ecol. Model.* **2019**, *392*, 92–102. [CrossRef]

4. Tsoka, S.; Tsikaloudaki, K.; Theodosiou, T.; Bikas, D. Urban warming and cities' microclimates: Investigation methods and mitigation strategies—A review. *Energies* **2020**, *13*, 1414. [CrossRef]
5. Tian, L.; Li, Y.C.; Lu, J.; Wang, J. Review on urban heat island in China: Methods, its impact on buildings energy demand and mitigation strategies. *Sustainability* **2021**, *13*, 762. [CrossRef]
6. Mathew, A.; Khandelwal, S.; Kaul, N. Spatial and temporal variations of urban heat island effect and the effect of percentage impervious surface area and elevation on land surface temperature: Study of Chandigarh city, India. *Sustain. Cities Soc.* **2016**, *26*, 264–277. [CrossRef]
7. Kiddle, G.L.; Pedersen Zari, M.; Blaschke, P.; Chanse, V.; Kiddle, R. An oceania urban design agenda linking ecosystem services, nature-based solutions, traditional ecological knowledge and wellbeing. *Sustainability* **2021**, *13*, 12660. [CrossRef]
8. Merodio Gómez, P.; Juarez Carrillo, O.J.; Kuffer, M.; Thomson, D.R.; Olarte Quiroz, J.L.; Villaseñor García, E.; Vanhuysse, S.; Abascal, Á.; Oluoch, I.; Nagenborg, M.; et al. Earth observations and statistics: Unlocking sociodemographic knowledge through the power of satellite images. *Sustainability* **2021**, *13*, 12640. [CrossRef]
9. Joshi, M.Y.; Teller, J. Urban integration of green roofs: Current challenges and perspectives. *Sustainability* **2021**, *13*, 12378. [CrossRef]
10. Valero, A.; Torrubia, J.; Anía, M.Á.; Torres, A. Assessing urban metabolism through MSW carbon footprint and conceptualizing municipal-industrial symbiosis—The case of Zaragoza city, Spain. *Sustainability* **2021**, *13*, 12724. [CrossRef]
11. Lobaccaro, G.; De Ridder, K.; Acero, J.A.; Hooyberghs, H.; Lauwaet, D.; Maiheu, B.; Sharma, R.; Govehovitch, B. Applications of models and tools for mesoscale and microscale thermal analysis in mid-latitude climate regions—A review. *Sustainability* **2021**, *13*, 12385. [CrossRef]
12. Lu, M.; Hou, T.Y.; Fu, J.W.; Wei, Y. The effects of microclimate parameters on outdoor thermal sensation in severe cold cities. *Sustainability* **2019**, *11*, 1572. [CrossRef]
13. Yang, Y.J.; Gatto, E.; Gao, Z.; Buccolieri, R.; Morakinyo, T.E.; Lan, H.N. The "plant evaluation model" for the assessment of the impact of vegetation on outdoor microclimate in the urban environment. *Build. Environ.* **2019**, *159*, 106151. [CrossRef]
14. Lenzholzer, S. Engrained experience-a comparison of microclimate perception schemata and microclimate measurements in Dutch urban squares. *Int. J. Biometeorol.* **2010**, *54*, 141–150. [CrossRef]
15. Zhen, M.; Dong, Q.; Chen, P.; Ding, W.; Zhou, D.; Feng, W. Urban outdoor thermal comfort in western China. *J. Asian Archit. Build.* **2021**, *20*, 222–236. [CrossRef]
16. Shooshtarian, S.; Lam, C.K.C.; Kenawy, I. Outdoor thermal comfort assessment: A review on thermal comfort research in Australia. *Build. Environ.* **2020**, *177*, 106917. [CrossRef]
17. Shooshtarian, S. Theoretical dimension of outdoor thermal comfort research. *Sustain. Cities Soc.* **2019**, *47*, 101495. [CrossRef]
18. Zhang, L.L.L.; Wei, D.; Hou, Y.Y.; Du, J.F.; Liu, Z.; Zhang, G.M.; Shi, L. Outdoor thermal comfort of urban park—A case study. *Sustainability* **2020**, *12*, 1961. [CrossRef]
19. Xue, J.; Gui, D.W.; Lei, J.Q.; Sun, H.W.; Zeng, F.J.; Mao, D.L.; Zhang, Z.W.; Jin, Q.; Liu, Y. Oasis microclimate effects under different weather events in arid or hyper arid regions: A case analysis in southern Taklimakan desert and implication for maintaining oasis sustainability. *Theor. Appl. Climatol.* **2019**, *137*, 89–101. [CrossRef]
20. Hao, X.M.; Li, W.H. Oasis cold island effect and its influence on air temperature: A case study of Tarim Basin, Northwest China. *J. Arid Land* **2016**, *8*, 172–183. [CrossRef]
21. Zhang, M.; Luo, G.P.; Hamdi, R.; Qiu, Y.; Wang, X.X.; De Maeyer, P.; Kurban, A. Numerical simulations of the impacts of mountain on oasis effects in arid central Asia. *Atmosphere* **2017**, *8*, 212. [CrossRef]
22. Bie, Q.; Xie, Y.W.; Wang, X.Y.; Wei, B.C.; He, L.; Duan, H.M.; Wang, J. Understanding the attributes of the dual oasis effect in an arid region using remote sensing and observational data. *Ecosyst. Health Sustain.* **2020**, *6*, 1096153. [CrossRef]
23. Yang, L.; Liu, X.D.; Qian, F. Research on water thermal effect on surrounding environment in summer. *Energy Build.* **2020**, *207*, 109613. [CrossRef]
24. Qiu, X.Y.; Kil, S.H.; Park, C. Impact of local environment on cooling island effect of water body: Case study of Changsha, China. *Sensor. Mater.* **2021**, *33*, 3801–3817. [CrossRef]
25. Zhang, J.; Gou, Z.H.; Lu, Y. Outdoor thermal environments and related planning factors for subtropical urban parks. *Indoor Built Environ.* **2021**, *30*, 363–374. [CrossRef]
26. Hathway, E.A.; Sharples, S. The interaction of rivers and urban form in mitigating the Urban Heat Island effect: A UK case study. *Build. Environ.* **2012**, *58*, 14–22. [CrossRef]
27. Zhou, X.F.; Zhang, S.; Zhu, D. Impact of urban water networks on microclimate and PM2.5 distribution in downtown areas: A case study of Wuhan. *Build. Environ.* **2021**, *203*, 108073. [CrossRef]
28. Xu, J.C.; Wei, Q.L.; Huang, X.F.; Zhu, X.Y.; Li, G.M. Evaluation of human thermal comfort near urban waterbody during summer. *Build. Environ.* **2010**, *45*, 1072–1080. [CrossRef]
29. Sun, R.; Chen, L. How can urban water bodies be designed for climate adaptation? *Landsc. Urban Plan.* **2012**, *105*, 27–33. [CrossRef]
30. Van Hove, L.W.A.; Jacobs, C.M.J.; Heusinkveld, B.G.; Elbers, J.A.; van Driel, B.L.; Holtslag, A.A.M. Temporal and spatial variability of urban heat island and thermal comfort within the Rotterdam agglomeration. *Build. Environ.* **2015**, *83*, 91–103. [CrossRef]
31. Steeneveld, G.J.; Koopmans, S.; Heusinkveld, B.G.; Theeuwes, N.E. Refreshing the role of open water surfaces on mitigating the maximum urban heat island effect. *Landsc. Urban Plan.* **2014**, *121*, 92–96. [CrossRef]

32. Zhou, D.; Xiao, J.; Bonafoni, S.; Berger, C.; Deilami, K.; Zhou, Y.; Frolking, S.; Yao, R.; Qiao, Z.; Sobrino, J.A. Satellite remote sensing of surface urban heat islands: Progress, challenges, and perspectives. *Remote Sens.* **2019**, *11*, 48. [CrossRef]
33. Mao, Q.; Peng, J.; Wang, Y. Resolution enhancement of remotely sensed land surface temperature: Current status and perspectives. *Remote Sens.* **2021**, *13*, 1306. [CrossRef]
34. Koehler, J.; Kuenzer, C. Forecasting spatio-temporal dynamics on the land surface using earth observation data—A review. *Remote Sens.* **2020**, *12*, 3513. [CrossRef]
35. Crommelinck, S.; Bennett, R.; Gerke, M.; Nex, F.; Yang, M.Y.; Vosselman, G. Review of automatic feature extraction from high-resolution optical sensor data for UAV-based cadastral mapping. *Remote Sens.* **2016**, *8*, 689. [CrossRef]
36. Vélez-Nicolás, M.; García-López, S.; Barbero, L.; Ruiz-Ortiz, V.; Sánchez-Bellón, Á. Applications of unmanned aerial systems (UASs) in Hydrology: A Review. *Remote Sens.* **2021**, *13*, 1359. [CrossRef]
37. Delavarpour, N.; Koparan, C.; Nowatzki, J.; Bajwa, S.; Sun, X. A technical study on UAV characteristics for precision agriculture applications and associated practical challenges. *Remote Sens.* **2021**, *13*, 1204. [CrossRef]
38. Cheng, L.; Guan, D.; Zhou, L.; Zhao, Z.; Zhou, J. Urban cooling island effect of main river on a landscape scale in Chongqing, China. *Sustain. Cities Soc.* **2019**, *47*, 101501. [CrossRef]
39. Li, X.T.; Yu, Z.; Zhao, B.; Li, Y. Numerical analysis of outdoor thermal environment around buildings. *Build. Environ.* **2005**, *40*, 853–866. [CrossRef]
40. Bo-Ot, L.M.; Wang, Y.H.; Chiang, C.M.; Lai, C.M. Effects of a Green Space Layout on the Outdoor Thermal Environment at the Neighborhood Level. *Energies* **2012**, *5*, 3723–3735. [CrossRef]
41. Yuan, J.H.; Farnham, C.; Emura, K. Effect of different reflection directional characteristics of building facades on outdoor thermal environment and indoor heat loads by CFD analysis. *Urban Clim.* **2021**, *38*, 100875. [CrossRef]
42. Ballinas, M.; Barradas, V.L. Transpiration and stomatal conductance as potential mechanisms to mitigate the heat load in Mexico City. *Urban For. Urban Green.* **2016**, *20*, 152–159. [CrossRef]
43. Wu, C.; Li, J.; Wang, C.; Song, C.; Chen, Y.; Finka, M.; La Rosa, D. Understanding the relationship between urban blue infrastructure and land surface temperature. *Sci. Total Environ.* **2019**, *694*, 133742. [CrossRef] [PubMed]
44. Anjos, M.; Lopes, A. Urban heat island and park cool island intensities in the coastal city of Aracaju, north-eastern Brazil. *Sustainability* **2017**, *9*, 1379. [CrossRef]
45. De Jesus, M.P.; Lourenço, J.M.; Arce, R.M.; Macias, M. Green façades and in situ measurements of outdoor building thermal behaviour. *Build. Environ.* **2017**, *119*, 11–19. [CrossRef]
46. Wong, N.H.; Chen, Y.; Ong, C.L.; Sia, A. Investigation of thermal benefits of rooftop garden in the tropical environment. *Build. Environ.* **2003**, *38*, 261–270. [CrossRef]
47. Lau, K.K.-L.; Ren, C.; Ho, J.; Ng, E. Numerical modelling of mean radiant temperature in high-density sub-tropical urban environment. *Energy Build.* **2016**, *114*, 80–86. [CrossRef]
48. Lin, T.-P.; Tsai, K.-T.; Liao, C.-C.; Huang, Y.-C. Effects of thermal comfort and adaptation on park attendance regarding different shading levels and activity types. *Build. Environ.* **2013**, *59*, 599–611. [CrossRef]
49. Takebayashi, H.; Moriyama, M. Relationships between the properties of an urban street canyon and its radiant environment: Introduction of appropriate urban heat island mitigation technologies. *Sol. Energy* **2012**, *86*, 2255–2262. [CrossRef]
50. Giannopoulou, K.; Santamouris, M.; Livada, I.; Georgakis, C.; Caouris, Y. The Impact of Canyon Geometry on Intra Urban and Urban: Suburban Night Temperature Differences Under Warm Weather Conditions. *Pure Appl. Geophys.* **2010**, *167*, 1433–1449. [CrossRef]
51. An, L.; Hong, B.; Cui, X.; Geng, Y.; Ma, X. Outdoor thermal comfort during winter in China's cold regions: A comparative study. *Sci. Total Environ.* **2021**, *768*, 144464. [CrossRef] [PubMed]
52. Xiong, J.; Yao, R.M.; Grimmond, S.; Zhang, Q.L.; Li, B.Z. A hierarchical climatic zoning method for energy efficient building design applied in the region with diverse climate characteristics. *Energy Build.* **2019**, *186*, 355–367. [CrossRef]
53. Mahgoub, A.O.; Gowid, S.; Ghani, S. Global evaluation of WBGT and SET indices for outdoor environments using thermal imaging and artificial neural networks. *Sustain. Cities Soc.* **2020**, *60*, 15. [CrossRef]
54. Cannistraro, M.; Trancossi, M. Enhancement of indoor comfort in the presence of large glazed radiant surfaces by a local heat pump system based on Peltier cells. *Therm. Sci. Eng. Prog.* **2019**, *14*, 12. [CrossRef]
55. Bruse, M.; Fleer, H. Simulating surface–plant–air interactions inside urban environments with a three dimensional numerical model. *Environ. Model. Softw.* **1998**, *13*, 373–384. [CrossRef]
56. Vaz Monteiro, M.; Doick, K.J.; Handley, P.; Peace, A. The impact of greenspace size on the extent of local nocturnal air temperature cooling in London. *Urban For. Urban Green.* **2016**, *16*, 160–169. [CrossRef]
57. Richards, D.R.; Fung, T.K.; Belcher, R.N.; Edwards, P.J. Differential air temperature cooling performance of urban vegetation types in the tropics. *Urban For. Urban Green.* **2020**, *50*, 126651. [CrossRef]
58. Shi, D.; Song, J.; Huang, J.; Zhuang, C.; Guo, R.; Gao, Y. Synergistic cooling effects (SCEs) of urban green-blue spaces on local thermal environment: A case study in Chongqing, China. *Sustain. Cities Soc.* **2020**, *55*, 102065. [CrossRef]
59. Theeuwes, N.E.; Solcerová, A.; Steeneveld, G.J. Modeling the influence of open water surfaces on the summertime temperature and thermal comfort in the city. *J. Geophys. Res.—Atmos.* **2013**, *118*, 8881–8896. [CrossRef]
60. Chow, W.T.L.; Pope, R.L.; Martin, C.A.; Brazel, A.J. Observing and modeling the nocturnal park cool island of an arid city: Horizontal and vertical impacts. *Theor. Appl. Climatol.* **2011**, *103*, 197–211. [CrossRef]

61. Xiao, Z.D.; Yang, C.; Liu, C.L.; Yang, L.M.; Yang, S.H.; Zhou, J.; Li, F.Q.; Jiang, L.W.; Xiao, S.; Gao, C.J.; et al. SINAT E3 ligases regulate the stability of the ESCRT component FREE1 in response to iron deficiency in plants. *J. Integr. Plant Biol.* **2020**, *62*, 1399–1417. [CrossRef] [PubMed]
62. Tsoka, S.; Tsikaloudaki, A.; Theodosiou, T. Analyzing the ENVI-met microclimate model's performance and assessing cool materials and urban vegetation applications—A review. *Sustain. Cities Soc.* **2018**, *43*, 55–76. [CrossRef]
63. Zhang, L.; Zhan, Q.; Lan, Y. Effects of the tree distribution and species on outdoor environment conditions in a hot summer and cold winter zone: A case study in Wuhan residential quarters. *Build. Environ.* **2018**, *130*, 27–39. [CrossRef]
64. Wang, Y.; Ouyang, W. Investigating the heterogeneity of water cooling effect for cooler cities. *Sustain. Cities Soc.* **2021**, *75*, 103281. [CrossRef]